n_{poss} = number of possible matches, defined by Equation (2)
ΔT_{min} = minimum approach temperature in a match (°C)
Cp = heat capacity flowrate (kW/°C)

Note:

All numerical values quoted are based on calculations using original data in Imperial units. Inevitable rounding on conversion to SI units may lead to small discrepancies.

LITERATURE CITED

Donaldson, R. A., "Studies in the Computer Aided Design of Complex Heat Exchange Networks," Ph.D. thesis, University of Edinburgh (1976).

Hohmann, E. C., "Optimum Networks for Heat Exchange," Ph.D. thesis, University of S. Calif. (1971).

Hohmann, E. C. and F. J. Lockhart, "Optimum Heat Exchanger Network Synthesis," Paper No. 22a, AIChE National Meeting, Atlantic City (1976).

Lee, K. F., A. H. Masso, and D. F. Rudd, "Branch and Bound Synthesis of Integrated Process Designs," *Ind. Eng. Chem. Fundam.*, 9, 48 (1970).

Linnhoff, B. and J. R. Flower, "Synthesis of Heat Exchanger Networks, I. Systematic Generation of Energy Optimal Networks, and II. Evolutionary Generation of Networks with Various Criteria of Optimality," *AIChE J.*, 24, 633 (1978).

Linnhoff, B., "Thermodynamic Analysis in the Design of Process Networks," Ph.D. thesis, Univ. of Leeds (1979).

Nishida, N., Y. A. Liu, and L. Lapidus, "Studies in Chemical Process Design and Synthesis: III. A Simple and Practical Approach to the Optimal Synthesis of Heat Exchanger Networks," *AIChE J.*, 23, 77 (1977).

Pho, T. and L. Lapidus, "Synthesis of Optimal Heat Exchanger Networks by Tree Searching Algorithms," *AIChE J.*, 19, 1182 (1973).

Ponton, J. W. and R. A. Donaldson, "A Fast Method for the Synthesis of Optimal Heat Exchanger Networks," *Chem. Eng. Sci.*, 29, 2375 (1974).

Manuscript received February 27, 1978; revision received May 11, 1979 and accepted July 23, 1979.

Axial Dispersion Through Tube Constrictions

DAVID W. WEAVER

and

JAMES S. ULTMAN

Department of Chemical Engineering
The Pennsylvania State University
University Park, PA 16802

Tracer gas dispersion was measured for laminar flow through three different tube constrictions, at orifice Reynolds numbers between 10 and 5000 and Schmidt numbers of 0.213 and 0.769. Each constriction generates a confined jet which significantly enhances axial dispersion at intermediate Reynolds numbers ranging from 100 to 1000.

SCOPE

In chronic lung diseases, such as bronchitis and asthma, there may be a pathological narrowing of airways due to abnormal mucous secretion, tissue inflammation, or a loss of tissue rigidity. Such a constriction may affect the transport of respired gases, both by its influence upon bulk flow and upon longitudinal mixing. In previous work we demonstrated how the dispersion of a tracer gas pulse is a convenient measurement of mixing in physical tube network models (Ultman and Blatman 1977) as well as in the human lung (Ultman et al. 1978). The object of the current work is to evaluate the effect of a constriction upon tracer gas dispersion in a single airway.

We employed three alternative models of an airway constriction, two sharp-edged orifices with hole-to-tube diameter ratios (β) of 0.2 and 0.5 and a tapering constriction with $\beta = 0.33$. Air flows corresponding to orifice Reynolds numbers (Re_o) from 10 to 5000 are investigated, with both helium (He) and pure oxygen (O_2) tracer gases. The results are expressed as the excess dispersion induced by the constriction relative to dispersion in the unconstricted tube.

CONCLUSIONS AND SIGNIFICANCE

In general, a tube constriction causes significant excess dispersion when $Sc < 1$ and when Re_o is in the range of 100 to 1000; below a critical orifice Reynolds number of approximately 600, the excess dispersion is an increasing function of Re_o. Above the critical value, it is a sharply decreasing function of Re_o. A Taylor-type analysis of the data verifies that the excess dispersion is caused by radial diffusion of tracer from a downstream orifice jet into the slowly circulating stall which it creates.

Address correspondence to: James Ultman, 106 Fenske Laboratory, University Park, PA 16802.

0001-1541-80-3130-0009-$00.95.

The magnitude of this excess dispersion is comparable to the tracer pulse dispersion previously measured in healthy human lungs. Thus, if pathological airway constrictions behave like the tube constrictions, it may be possible to detect them with a tracer pulse-response technique.

Several tests of pulmonary function, notably the nitrogen wash-out procedure (Baker, Ultman and Rhoades 1975), are influenced by longitudinal gas mixing in the conducting airways. In a healthy lung, these airways are essentially cylindrical tube segments. Lung disease can cause narrowing of the airways, affecting both the flow resistance and the mixing of respired gases. Thus the improvement of existing diagnostic procedures as well as the development of new function tests depends upon our understanding of how airway constriction influences gas mixing. The purpose of this work is to measure and analyze axial mixing in physical models of pathological airway constrictions and compare the results to mixing in unconstricted airways.

Developing a unique physical model is not possible, since the anatomy of an airway constriction is probably variable, depending on the nature and the severity of the lung disease. Therefore, we selected two different geometries to study. The VDI standard orifice (Streeter 1971) is a sharp-edged constriction, while the M-2 model of Morgan and Young (1974) is a tapering constriction whose boundaries trace out a cosine function (Figure 1).

In spite of the difference in the severity of the two constrictions, the associated fluid mechanics are remarkedly similar. While the flow is completely streamlined upstream of the M-2 constriction, the sharp change of fluid direction in the upstream corner of the orifice constriction causes a minor degree of fluid detachment and circulation (Johansen 1929). Downstream of both types of constrictions, a confined jet is formed. Shear forces at the boundary of the jet causes it to progressively entrain fluid and widen until, at $X = X_a$, the jet reattaches to the tube wall. The region between the jet boundary and the tube wall is filled with a slowly circulating vortex or stall of fluid.

This stall acts as a dead volume into which solute from the jet is transported by radial diffusion. In this manner, dispersion may be enhanced by the presence of a constriction. The degree of enhancement is proportional to the volume of the stall and, therefore, to the reattachment length (X_a) of the jet. At low Reynolds numbers, when the jet is laminar, its length is directly proportional to Re_o; above a critical value of Re_o, flow at the jet boundary becomes turbulent and X_a is a decreasing function of the Reynolds number. The stall is largest at the critical Reynolds number. We expect that the enhancement of dispersion will similarly be maximized at a critical Reynolds number.

In this work, single pulses of pure oxygen and of pure helium are injected into flowing air to study the enhancement of dispersion by two standard orifices ($\beta = 0.2$ and 0.5) and by the M-2 tapering constriction ($\beta = 0.33$)

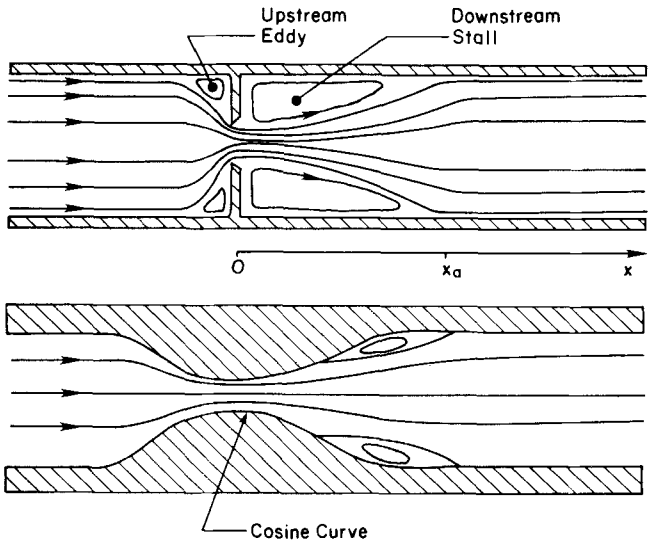

Figure 1. Streamlines of flow through a standard sharp-edged orifice (top) and an M-2 tapered constriction (bottom). The constrictions are centered at $X = 0$ and the confined jet reattaches to the tube wall at $X = X_a$.

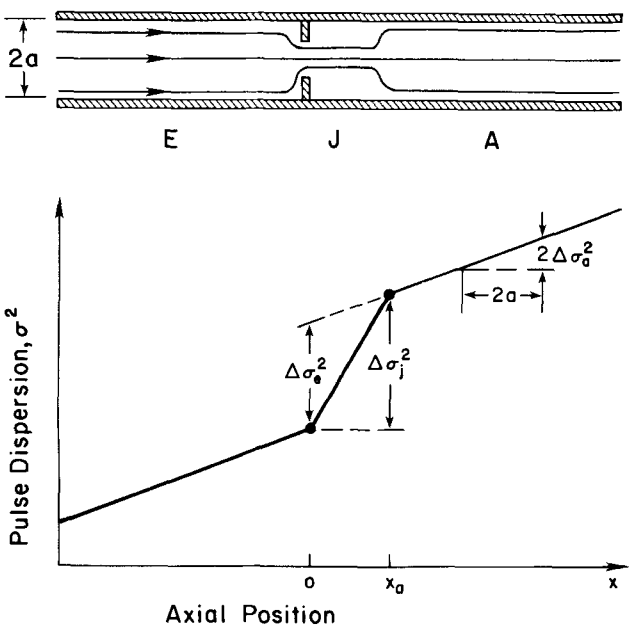

Figure 2. Idealized streamlines of flow (top) and pulse dispersion (bottom) through the constriction test section. The velocity and concentration profiles are fully-developed in the entrance [*E*], jet [*J*], and after [*A*] regions and the confined jet is cylindrical. The absolute dispersion ($\Delta\sigma_J^2$) and excess dispersion ($\Delta\sigma_e^2$) of the jet region are shown.

over a Re_o range of 10 to 5000. A Taylor-type dispersion theory is developed as a first-order explanation of the laminar dispersion data.

THEORY

For simplicity, we visualize the constriction test section (Figure 2) as being comprised of a confined jet region (J) surrounded by an entrance region (E) and an after region (A). Axial mixing in any of these regions may be characterized by a mixing coefficient (D). If D is constant, then the tracer pulse dispersion (σ^2) will be a linear function of axial position (X) provided that end effects are negligible. In such regions (Levenspiel and Smith 1957),

$$\sigma^2 = \frac{2X}{u^3} D \tag{1}$$

where u is the mean axial velocity. In order to simplify theoretical analysis, we consider both velocity and tracer concentration profiles to be fully-developed throughout the test section. Then the mixing coefficients in regions E and A are both equal to the same constant value (D_∞) and the coefficient (D_J) in region J is also constant. We employ Equation (1) to define the excess dispersion ($\Delta\sigma_e^2$) induced by the constriction in region J as

$$\Delta\sigma_e^2 \equiv \frac{2X_a}{u^3} (D_J - D_\infty) \tag{2}$$

Also, we characterize mixing in the unconstricted tube by the increase in dispersion ($\Delta\sigma_a^2$) that occurs over an axial distance equal to the tube radius (a).

$$\Delta\sigma_a^2 = \frac{2a}{u^3} (D_\infty) \tag{3}$$

We now define the enhancement factor (Φ_a) as the ratio of $\Delta\sigma_e^2$ to $\Delta\sigma_a^2$.

$$\Phi_a \equiv \frac{\Delta\sigma_e^2}{\Delta\sigma_a^2} = \frac{X_a}{a}\left(\frac{D_J}{D_\infty} - 1\right) \tag{4}$$

This factor represents the number of radii of unobstructed tube length necessary to cause a pulse dispersion equal to the excess dispersion of the constriction.

The formulation of D_∞ is available (Taylor 1953)

$$D_\infty = \mathcal{D} + \frac{u^2a^2}{48\mathcal{D}} \tag{5}$$

but D_J will be derived from a Taylor-type analysis. We begin by idealizing the velocity field (u_x) in region J as

$$u_x = \begin{cases} u/\beta^2; & \beta a \geq r \geq 0 \text{ (jet)} \\ 0 & a \geq r > \beta a \text{ (stall)} \end{cases} \tag{6}$$

where r is the radial position. In other words, we assume that the jet has a uniform velocity profile and a cylindrical boundary. The radius of the jet is taken to be that of the constriction and the surrounding stall is assumed to be quiescent. Taylor's conservation equation for the local tracer concentration ($\overline{C}$) is

$$[u_x - u]\frac{\partial\overline{C}}{\partial X_1} - \mathcal{D}\left[\frac{1}{r}\frac{\partial}{\partial r}\left(r\frac{\partial\overline{C}}{\partial r}\right)\right] = 0 \tag{7}$$

and, in addition,

$$\left[\frac{\partial\overline{C}}{\partial r}\right]_{r=0} = \left[\frac{\partial\overline{C}}{\partial r}\right]_{r=a} = 0 \tag{8}$$

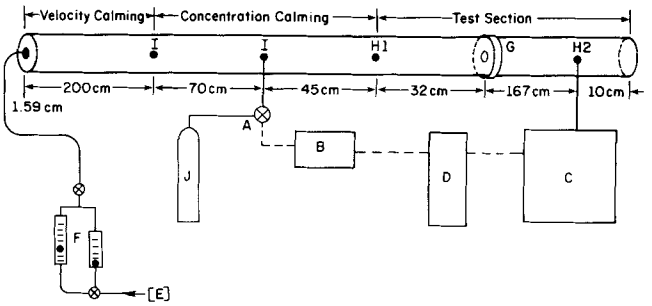

Figure 3. Schematic diagram of the experimental system. Tubing and electrical connections are indicated by the solid and the broken curves, respectively. The alphabetic designations are explained in the text.

where

$$X_1 \equiv X - ut$$

and $(\partial\overline{C}/\partial X_1)$ is considered to be a function of X_1 only. The solution to Equations (7) and (8) for the velocity field given by Equation (6) is

$$\overline{C} = \begin{cases} [\overline{C}]_{r=0} + \dfrac{u}{4\mathcal{D}}[\beta^{-2} - 1]r^2\dfrac{\partial\overline{C}}{\partial X_1}; & \beta a \geq r \geq 0 \\ [\overline{C}]_{r=a} + \dfrac{u}{4\mathcal{D}}[a^2 - r^2 + 2a^2\ln(r/a)]\dfrac{\partial\overline{C}}{\partial X_1}; & a \geq r > \beta a \end{cases} \tag{9}$$

If we also note that $\overline{C}$ must be continuous at $r = \beta a$, then

$$[\overline{C}]_{r=a} = [\overline{C}]_{r=0} - 2a^2\ln\beta\frac{\partial\overline{C}}{\partial X_1} \tag{10}$$

The flux (J_x) of tracer relative to a fixed X_1 coordinate can be computed from the definition

$$J_x \equiv \frac{2}{a^2}\int_0^a \overline{C}[u_x - u]r\,dr \tag{11}$$

and the Taylor dispersion coefficient is defined as the ratio of J_x to $-(\partial\overline{C}/\partial X_1)$. Then combining Equations (9, 10) and (11) we find that

$$\left[J_x \Big/ \left(-\frac{\partial\overline{C}}{\partial X_1}\right)\right] = \frac{u^2a^2}{4\mathcal{D}}(\beta^2 - 1 - 2\ln\beta) \tag{12}$$

After adding $\mathcal{D}$ in order to account for axial diffusion, the mixing coefficient of the jet is obtained.

$$D_J = \mathcal{D} + \frac{u^2a^2}{4\mathcal{D}}(\beta^2 - 1 - 2\ln\beta) \tag{13}$$

Finally, combining Equations (4, 5) and (13) results in a theoretical expression for the enhancement factor.

$$\Phi_a = \left[\left(\frac{X_a}{a}\right)\left(\frac{\beta Re_o Sc}{4}\right)^2\left(\beta^2 - \frac{13}{12} - 2\ln\beta\right)\right]\left[1 + \frac{1}{3}\left(\frac{\beta Re_o Sc}{8}\right)^2\right]^{-1} \tag{14}$$

At orifice Reynolds numbers below the critical value, the confined jet is laminar and its point of reattachment is proportional to Re_o. That is,

$$(X_a/a) = \alpha Re_o \tag{15}$$

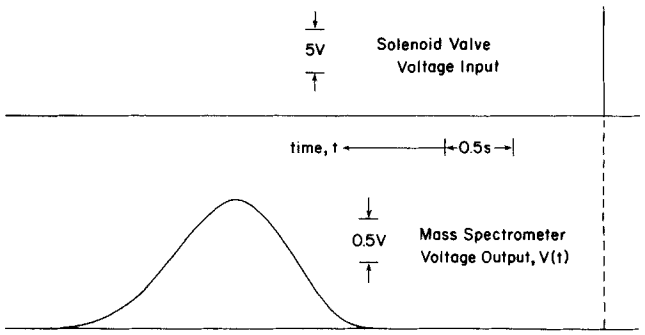

Figure 4. Strip chart recording for a helium pulse. The time scale of the breakthrough curve (bottom) is referenced to the triggering of the solenoid valve (top).

where the proportionality function α depends upon the nature of the constriction as well as the particular value of β. In that case

$$\Phi_a = \frac{\alpha(\beta Sc)^2 Re_o^3}{16}\left(\beta^2 - \frac{13}{12} - 2\ln\beta\right)\Big/ \left[1 + \frac{(\beta Sc Re_o)^2}{192}\right] \quad (16)$$

When Re_o exceeds its critical value, then the jet boundary becomes turbulent so that X_a is inversely related to Re_o. In that case, Equation (14) predicts that Φ_a decreases with increasing Re_o.

EXPERIMENTAL METHODS

The experimental system (Figure 3) was designed so as to provide fully-developed velocity and concentration profiles to the test section. Therefore the constriction [G] is positioned in a test section which is preceded by velocity and concentration calming sections. The length of tubing (L_c) for concentration calming is estimated as

$$(L_c/a) = 0.25\, ReSc \quad (17)$$

where Re is the tube Reynolds number. Two 1.6 mm holes, serving as alternative tracer injection sites [I] are located 45 and 115 cm upstream of the first sampling port [H1]. For experimental conditions such that $L_c < 45$ cm, the tracer is injected into the downstream monitoring port, while the upstream port is used when 115 cm $\geq L_c \geq$ 45 cm. The maximum entrance length (L_v) for velocity profile development occurs at a Re value of 2100. Judging from the equation,

$$(L_v/a) = 0.1\, Re \quad (18)$$

a value of 200 cm was more than sufficient for the length of the velocity calming section.

Filtered and humidified air [E] was introduced into the horizontal plastic tubing system which has an inside diameter of 1.59 cm and a total length of 524 cm. The air flow could be metered in the range 1-500 mL/sec, using high and low sensitivity rotometers [F]. Seventeen 0.8 mm holes, located 32, 17, 7, and 2 cm upstream and 2, 7, 17, 32, 47, 62, 77, 92, 107, 122, 137, 152 and 167 cm downstream of the center of the constriction, serve as concentration sampling ports. The tubing extends 10 cm beyond the last sample port [$H2$] to prevent artifacts due to diffusion from the atmosphere.

Tracer gas was injected through a 1.6 mm o.d. stainless steel capillary tube inserted perpendicularly into the injection port; the capillary is plugged at the bottom and perforated with nine 0.6 mm holes distributed uniformly around the capillary. With this hole distribution, a radially uniform slug of tracer could be delivered from a com-

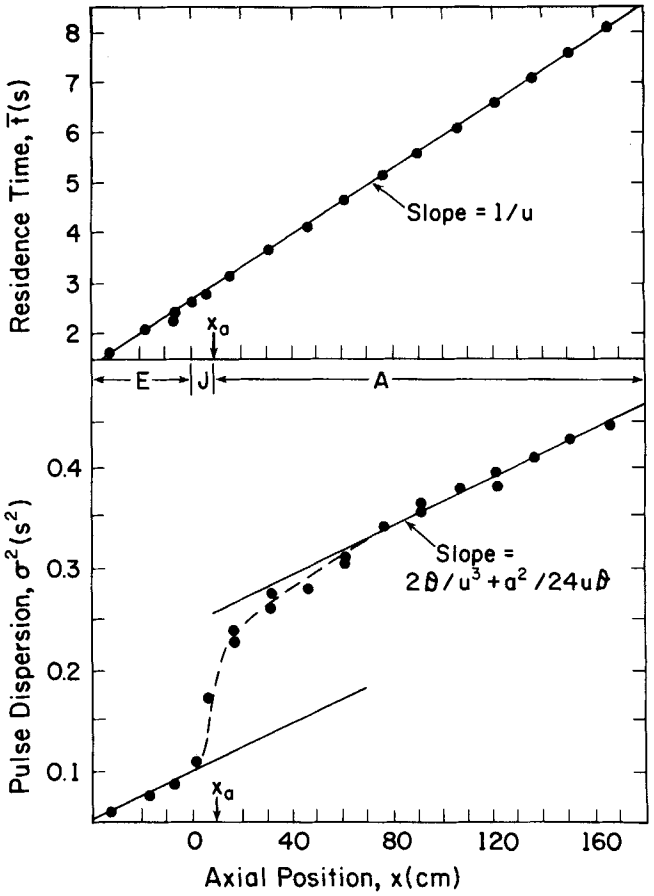

Figure 5. Residence time (top) and helium pulse dispersion (bottom) data for the $\beta = 0.5$ standard sharp-edged orifice when $Re_0 = 650$. The value of X_a was computed with Eq. 15 using an $\alpha = 0.05$ (Macagno and Hung 1966).

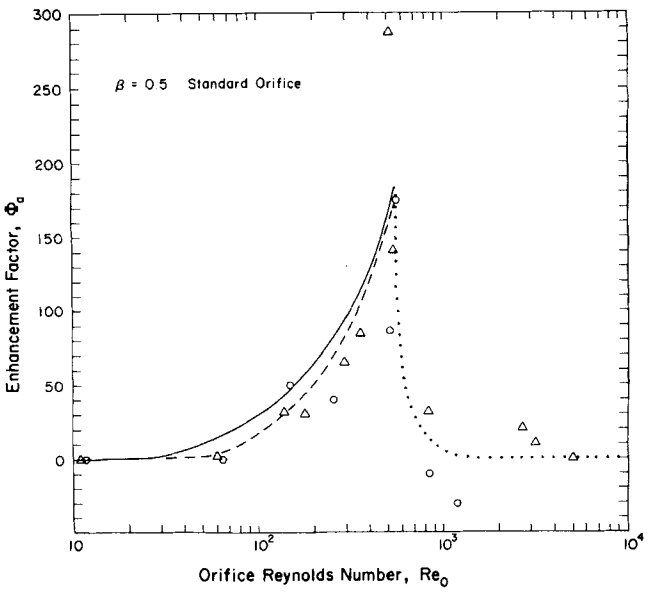

Figure 6. Enhancement of pulse dispersion for the $\beta = 0.5$ standard sharp-edged orifice. The helium (△) and oxygen (○) data as well as the helium (– – –) and oxygen (——) laminar jet dispersion theory are shown. The dotted curve (. . . .) indicates the trend of the turbulent jet dispersion data but has no theoretical basis.

pressed gas cylinder [J] through a 2-way subminiature solenoid valve [A]. This valve, which had a response time of 3 msec., could be pulsed electronically [B] for any duration in the range 3-125 msec. For most experiments, a 30 msec pulse duration at a compressed gas pressure of 10 psig (68.95 kPa) is employed, but at airflows less than 10 mL/sec, it was necessary to increase the duration to 100 msec and decrease the pressure to 1 psig (6.895 kPa) to obtain a smooth tracer concentration signal.

The point concentration of tracer is continuously determined by a mass spectrometer [C] (RMS-3; McGaw Respiratory Therapy) from a 0.5 mL/sec stream of gas which was withdrawn from the centerline of the test section through a 25 gauge hypodermic needle. The mass spectrometer exhibited a 200 msec transport delay and a 90% step response of 90 msec; since we are concerned with the difference in pulse dispersion between two sampling points, the effects of the mass spectrometer dynamics are largely cancelled out. The voltage output of the mass spectrometer and the input voltage to the solenoid were connected to two channels of a fast responding (60 Hz) strip chart recorder [D] (Brush 280; Gould, Inc.).

Both He and pure O_2 are used as tracers, but always in separate experiments. When oxygen is the tracer, the zero suppression on the strip-chart recorder is adjusted to eliminate the ambient O_2 signal from the concentration record. Experiments were performed over a *laminar Re range* of 4 to 2,100, using the sharp-edged orifices and the M-2 tapering constriction. During an experiment a breakthrough curve (Figure 4) is obtained at each of several sampling ports along the tube. In order to use Equation (1) to determine how σ^2 varied with x, the pulses delivered at the injection port had to be identical; duplicate breakthrough curves obtained at each sampling port do indicate that pulse delivery is reproducible.

Each breakthrough curve is analyzed to determine the mean residence time, relative to the time of tracer pulse injection,

$$\bar{t} \equiv \int_0^\infty tV(t)dt \Big/ \int_0^\infty V(t)dt \qquad (19)$$

and the tracer dispersion,

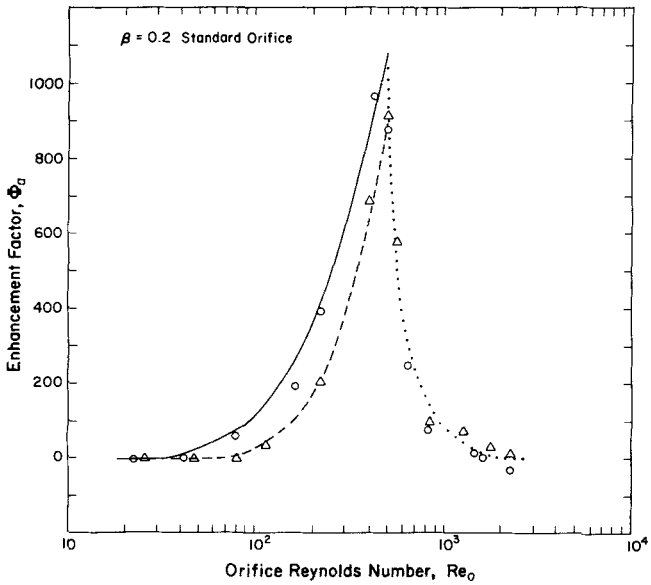

Figure 7. Enhancement of pulse dispersion for the $\beta = 0.2$ standard sharp-edged orifice.

$$\sigma^2 \equiv \int_0^\infty t^2V(t)dt \Big/ \int_0^\infty V(t)dt - \bar{t}^2 \qquad (20)$$

where $V(t)$ is the time dependent mass spectrometer signal. The integrals in Equations (19) and (20) are computed by employing Simpson's rule. The values of $\bar{t}$ and σ^2 of all samples are then plotted as a function of axial position, X. In all calculations, the kinematic viscosity (ν) of the tracer-air mixture was taken as 0.149 cm^2/s and the molecular diffusivities of He and O_2 in air were 0.698 and 0.194 cm^2/s, respectively.

COMPARISON OF THE DATA AND THEORY

Since they were obtained from sampling sites consistently located at the tube centerline, the increase in $\bar{t}$ and in σ^2 values with axial position (Figure 5) is identical to that associated with the area-averaged tracer concentration (Ultman and Weaver 1979) which is the basis of the dispersion theory. The results of Levenspiel and Smith (1957) indicate that, in a region free of end effects (i.e., where $uX/D >> 1$), the tracer breakthrough curve is symmetric about $\bar{t}$, and both the $\bar{t} - X$ and $\sigma^2 - X$ plots are linear, having slopes of $1/u$ and $2D/u^3$, respectively. Although the typical breakthrough curve (Figure 4) is not absolutely symmetrical, its degree of skewness is not sufficient to upset the linearity of the $\bar{t} - X$ plot. The lack of importance of end effects is also demonstrated by the linearity of the $\sigma^2 - X$ plot throughout region E and in the downstream portion of region A, where the disturbance of the confined jet has been dissipated. In fact, these two linear segments are parallel and have slopes which are in accord (to within 5%) with the Taylor dispersion theory (Equation 5). Within region J, the $\sigma^2 - X$ data is non-linear because, as discussed in the next section, the velocity and concentration profiles are not fully-developed and thus D_J is dependent upon X.

The trends of Φ_a, computed from the $\sigma^2 - X$ data as the quotient of $\Delta\sigma_e^2$ and $\Delta\sigma_a^2$ (Figure 2), are similar for the standard orifices (Figures 6 and 7) and for the M-2 constriction (Figure 8). The enhancement factor rises above zero when the orifice Reynolds number is greater than 60. As Re_o is increased, Φ_a also increases until it reaches a maximum value of several hundred. The critical Re_o at which this maximum is reached has a value of 500 for both standard orifices and 800 for the M-2 constriction. Beyond the critical Re_o, Φ_a falls off sharply to zero. For values of Re_o greater than 1000, some negative values of Φ_a were observed.

The ascending portion of the $\Phi_a - Re_o$ curves are caused by the increased volume of the dead zone that accompanies lengthening of the laminar jet. For the $\beta = 0.5$ orifice, where $\alpha = 0.05$, the theory (Equation 16) follows the correct trend but somewhat overestimates the data. Using an α value of 0.045 deduced from Morgan and Young's (1974) hydrodynamic theory, we find that the theoretical $\Phi_a - Re_o$ curves constructed for the M-2 constriction agree quite well with the data (Figure 8).

For the $\beta = 0.5$ orifice and the M-2 tapering constriction, any systematic difference between the He and the O_2 data is obscured by the lack of precision. This is apparent if one compares the small difference between the theoretical curve for O_2 and He to the relatively large scatter of the data points. On the ascending portion of Figure 7, however, the Φ_a data points for O_2 appear to be significantly greater than those for He. To see whether this differential could be explained by the theory, we performed a least square regression of the $\beta = 0.2$

orifice data with Equation 16. Using the resulting value of 0.087 for α, the "theoretical" curves in Figure 6 were produced. The differential between the O_2 and the He data is indeed consistent with that anticipated by the theory. Also, by comparing α values for the $\beta = 0.2$ and $\beta = 0.5$ orifices, it appears that α is inversely proportional to β.

The initiation of the descending portion of all the $\Phi_a - Re_o$ curves is associated with the onset of turbulence at a critical Reynolds number. For the $\beta = 0.5$ orifice a critical Re_o of 350 was previously determined (Iribarne et al. 1972) by flow visualization experiments; this is in rough agreement with the critical value exhibited in Figure 6. The length of a turbulent jet is actually a decreasing function of Re_o which explains why Φ_a falls to zero as Re_o is increased beyond its critical value. The occasional negative Φ_a values that occur when $Re_o >$ 1,000 may reflect the fact that mixing in the jet region is dominated by turbulent dispersion. Since the turbulent dispersion coefficient is generally smaller than the laminar Taylor coefficient (Taylor 1954), Φ_a can indeed become negative (i.e., $D_J < D_*$ in Equation 2).

LIMITATIONS OF THE THEORY

The theory neglects the circulation of fluid in the stall. Johansen (1929) observed that, near the tube wall and at an Re_o of 150, the stall velocity is one-fifth of the jet velocity. Taking the circumference of the circulating stall to be twice the length of the jet, we estimate a circulation time of $10X_a\beta^2/u$. Since the time constant for radial diffusion is 0.5 $a^2/\mathcal{D}$, the ratio of the radial diffusion rate to the circulation rate is $(40\alpha\beta/\mathrm{Sc})$. For the $\beta = 0.5$ orifice, the reattachment parameter α has a known value of 0.05 (Macagno and Hung 1966). Thus helium dispersion through this orifice has a diffusion-to-circulation rate ratio of 4.7, and the assumption of a quiescent stall region is reasonable. The value of the ratio for oxygen is, however, only 1.3, and thus convection in the stall will affect the axial dispersion. Since tracer near the jet boundary has a positive local velocity while tracer near the tube wall is convected upstream, it is possible for the stall circulation to cause more axial dispersion than the theory predicts.

It should be noted that for liquid solvents, where Sc is generally large, $(40 \propto \beta/Sc) << 1$ so that very little tracer will diffuse into the stall region and we would not expect axial dispersion to be enhanced.

The theory also assumes that the velocity and concentration profiles are fully-developed within the jet. Employing Equation (15) and Equations (17) and (18), as applied to the jet, we compute the ratio of L_v to X_a as $0.1/\alpha$ and the ratio of L_c to X_a as $0.25\ Sc/\alpha$. Thus, for the $\beta = 0.5$ orifice the velocity entrance length is one-half the jet length while the concentration entrance length for helium and oxygen are, respectively, 0.26 and 0.94 times the jet length. Therefore, profiles will not be fully-developed over the entire jet length and dispersion will be less than is predicted by the theory, especially for O_2.

While the jet is taken to be cylindrical in the theoretical analysis, it must in reality begin to diverge at a finite distance upstream of the reattachment point. Therefore the "mean" radius of the jet is somewhat larger than that of the orifice and dispersion will be somewhat less than is predicted by the theory.

Although it is prohibitively difficult to evaluate the relative importance of these effects, it is quite possible

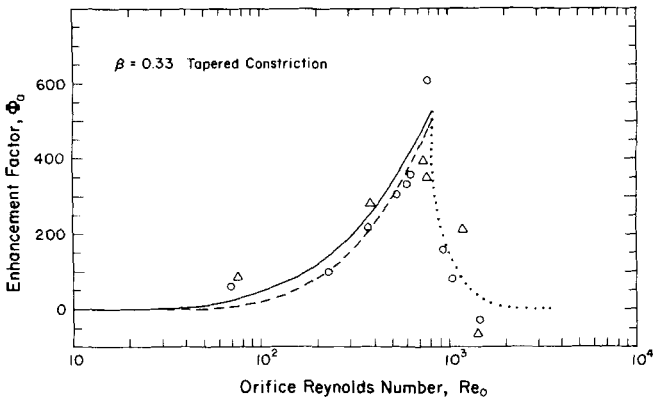

Figure 8. Enhancement of pulse dispersion for the $\beta = 0.33$ M-2 tapered constriction.

that the close fit of the theory to the subcritical enhancement data is due to a cancellation of the overestimations made by assuming a cylindrical jet and fully-developed profiles, with the underestimation caused by assuming a quiescent stall region.

RELEVANCE TO PULMONARY FUNCTION

In a previous study (Ultman et al. 1978), we measured the dispersion of helium pulses in normal human subjects. In each experiment, the seated subject inspired and expired a 700 ml volume of air at a constant inspiratory and expiratory flow rate of 400 mL/s. At a predetermined

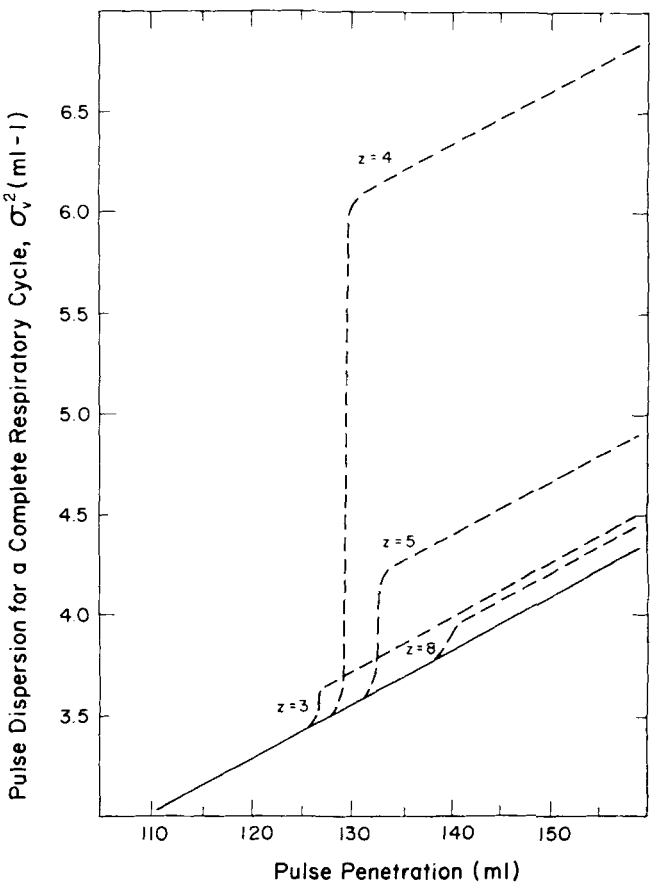

Figure 9. Estimated helium pulse dispersion (– – –) in the human lung for a $\beta = 0.5$ constriction located in airway generation z of Weibel's model 'A'. The respiratory flow rate is 400 mL/s and the solid line (——) is the dispersion measured in a healthy lung (Ultman et al. 1978).

lung volume relative to the end of inspiration, termed the penetration volume (V_p), a 20 mL pulse of helium was automatically injected into the inspired air. Since the tracer gas composition as well as the respired air volume was monitored throughout this inspiration and the following expiration, it was possible to compute the increase in dispersion throughout a single respiratory cycle. Because there was necessarily some variation in the flow, the dispersion was expressed as the variance of tracer concentration with respect to respired air volume (σ_v^2). Figure 9 indicates the relationship between penetration volume and σ_v^2.

To estimate the effect of an airway constriction on this pulmonary pulse dispersion, we employed Weibel's (1963) geometric model 'A' of the lung airway system. The model consists of a tube network wherein each tube of generation z branches into 2 identical tubes of generation $z + 1$. Generation zero contains one tube (i.e., the trachea), followed by 23 generations of successive branching which terminate in the elastic sacs through which oxygen and carbon dioxide are exchanged with the bloodstream. Each generation, therefore, contains 2^z tubes of equal length and equal radius.

If an identical constriction appeared in every branch of a particular generation, the total lung dispersion would be

$$(\sigma_v^2)_{\text{constriction}} = (\sigma_v^2)_{\text{unconstricted}} + 2\dot{V}^2\Delta\sigma_J^2 \quad (21)$$

where $\Delta\sigma_J^2$ is the dispersion (in s^2) through each branch. The factor of 2 accounts for the fact that respiration is bi-directional and $\dot{V}$ is the rate of air flow through the trachea. Using Figure 6 and the geometric dimensions prescribed by Weibel's model in order to compute $\Delta\sigma_J^2$, we estimated the total lung dispersion for a $\beta = 0.5$ constriction that is alternatively located in the third, fourth, fifth and eighth generation. The results, even for this large orifice, suggest that patients with a partial airway obstruction will exhibit a measurable enhancement of dispersion. In fact, at any specified respired flow, there is a constriction location at which the enhancement is maximized. For example, Figure 9 demonstrates that for a $\beta = 0.5$ orifice and $\dot{V} = 400$ mL/s, the enhancement is maximized when the constriction is located at the fourth generation.

ACKNOWLEDGMENTS

This work was supported in part by National Institutes of Health Grant HL 20347 and National Science Foundation Grant ENG75-04351. The assistance of Lisa Tweed in obtaining the M-2 constriction data is appreciated.

NOTATON

a = tube radius (cm)
$\bar{C}$ = local tracer concentration (mL tracer/mL gas)
D, D_x, D_J = axial mixing coefficient in general, in the unconstricted tube, and in the jet region, respectively (cm^2/s)
$\mathcal{D}$ = molecular diffusivity of the tracer gas in air (cm^2/s)
L_v, L_c = length of tubing required for a fully-developed velocity profile and concentration profile, respectively (cm)
J_x = axial tracer flux relative to the mean velocity (mL tracer/cm^2/s)
r = radial position (cm)
Re, Re_o = Reynolds number based upon the tube radius and the constriction radius, respectively ($Re = \beta Re_o = 2\,ua/\nu$)
Sc = Schmidt number ($\nu/\mathcal{D}$)
$t, \bar{t}$ = clock time and mean residence time, respectively (s)
u_x, u = local axial velocity and mean axial velocity, respectively (cm/s)
V = mass spectrometer output (volts)
X, X_1 = axial position relative to the center of the constriction and relative to the center of mass of the tracer pulse, respectively (cm)
X_a = value of X where jet reattachment occurs (cm)
z = airway generation counting from the trachea which is taken as $z = 0$

Greek Letters

α = reattachment factor for a laminar confined jet (Eq. 15)
β = ratio of constriction radius to tube radius
ν = kinematic viscosity (cm^2/s)
Φ_a = dispersion enhancement factor (Eq. 4)
σ^2, σ_v^2 = dispersion with respect to time and with respect to respired volume, respectively (s^2 and ml-1, respectively)
$\Delta\sigma_a^2, \Delta\sigma_J^2$ = dispersion over length a in the unconstricted tube and over the jet region, respectively (s^2)
$\Delta\sigma_e^2$ = excess dispersion in the jet region (s^2)

LITERATURE CITED

Baker, L., J. Ultman and R. Rhoades, "Characterization of Lung Geometry from the Single-Breath Nitrogen Washout Test," *Comp. Biomed. Res.*, **8**, 254-266 (1975).

Iribarne, A., F. Frantisak, R. L. Hummel and J. W. Smith, "An Experimental Study of Instabilities and Other Flow Properties of a Laminar Pipe Jet," *AIChE J.*, **18**, 689-698 (1972).

Johansen, F. C., "Flow Through Pipe Orifices at Low Reynolds Numbers," *Proc. Roy. Soc.*, **126A**, 231-245 (1929).

Levenspiel, O. and W. K. Smith, "Notes on the Diffusion-Type Model for the Longitudinal Mixing of Fluids in Flow," *Chem. Eng. Sci.*, **6**, 227-233 (1957).

Macagno, E. O. and T. K. Hung, "Computational and Experimental Study of a Captive Annular Eddy," *J. Fluid Mech.*, **28**, 43-64 (1967).

Morgan, B. E. and D. F. Young, "An Integral Method for the Analysis of Flow in Arterial Stenoses," *Bull. Math. Biol.*, **36**, 39-53 (1974).

Streeter, V. L., *Fluid Mechanics*, McGraw-Hill, New York (1971).

Taylor, G. I., "Dispersion of Soluble Matter in Solvent Flowing Slowly Through a Tube," *Proc. Roy. Soc.*, **219A**, 186-203 (1953).

Taylor, G. I., "The Dispersion of Matter in Turbulent Flow Through a Pipeline," *Proc. Roy. Soc.*, **223A**, 446-466 (1954).

Ultman, J. S. and D. W. Weaver, "Concentration Sampling Methods in Relation to the Determination of Dispersion Coefficients," *Chem. Eng. Sci.*, **34**, 1170-1172 (1979).

Ultman, J. S. and Hal S. Blatman, "A Compartmental Dispersion Model for the Analysis of Mixing in Tube Networks," *AIChE J.*, **23**, 169-176 (1977).

Ultman, J. S., B. E. Doll, R. Spiegel, and M. W. Thomas, "Longitudinal Mixing in Pulmonary Airways—Normal Subjects Respiring at a Constant Flow," *J. Appl. Physiol.: Respirat. Environ. Exercise Physiol.*, **44**, 297-303 (1978).

Weibel, E., *Morphometry of the Human Lung*, Chap. 11, Academic Press, New York (1963).

Manuscript received January 19, 1978; revision received July 10, and accepted July 23, 1979.